

Forces from stochastic density functional theory under nonorthogonal atom-centered basis sets

Ben Shpiro

*Fritz Haber Center for Molecular Dynamics and Institute of Chemistry,
The Hebrew University of Jerusalem, Jerusalem 9190401, Israel*

Marcel David Fabian

*Fritz Haber Center for Molecular Dynamics and Institute of Chemistry,
The Hebrew University of Jerusalem, Jerusalem 9190401, Israel*

Eran Rabani*

*Department of Chemistry, University of California, Berkeley, California 94720, USA
Materials Sciences Division, Lawrence Berkeley National Laboratory, Berkeley, California 94720, USA and
The Raymond and Beverly Sackler Center of Computational Molecular
and Materials Science, Tel Aviv University, Tel Aviv 69978, Israel*

Roi Baer†

*Fritz Haber Center for Molecular Dynamics and Institute of Chemistry,
The Hebrew University of Jerusalem, Jerusalem 9190401, Israel*

We develop a formalism for calculating forces on the nuclei within the linear-scaling stochastic density functional theory (sDFT) in a nonorthogonal atom-centered basis set representation (Fabian et al. WIREs Comput Mol Sci. 2019;e1412. <https://doi.org/10.1002/wcms.1412>) and apply it to Tryptophan Zipper 2 (Trp-zip2) peptide solvated in water. We use an embedded-fragment approach to reduce the statistical errors (fluctuation and systematic bias), where the entire peptide is the main fragment and the remaining 425 water molecules are grouped into small fragments. We analyze the magnitude of the statistical errors in the forces and find that the systematic bias is of the order of 0.065 eV/\AA ($\sim 1.2 \times 10^{-3} E_h/a_0$) when 120 stochastic orbitals are used, independently of systems size. This magnitude of bias is sufficiently small to ensure that the bond lengths estimated by stochastic DFT (within a Langevin molecular dynamics simulation) will deviate by less than 1% from those predicted by a deterministic calculation.

I. INTRODUCTION

Kohn-Sham density functional theory (KS-DFT) is often used for estimating the forces on the nuclei in *ab-initio* molecular dynamics simulations, with which reliable predictions concerning structure and properties of molecules can be made. Despite the fact that it can be used to study extended molecular systems relevant to biomolecular chemistry and materials science,[1–4] the conventional applications are limited in size due to the cubic algorithm complexity. Therefore, several approaches to KS-DFT have been developed and are routinely used for treating such extended systems. These include linear-scaling approaches which rely on electron localization within the system’s interior volume,[5–33] or the tight-binding DFT approach, which uses a very small basis set complemented by approximations calibrated with empirical data,[34–36] and the orbital-free DFT, which is applicable to relatively homogeneous systems.[37, 38] The way many of the linear scaling approaches achieve their gentle algorithmic complexity in-

volves imposing a sparse structure on the KS density matrix (DM) in a local real-space basis representation, effectively truncating the protruding elements. The rationale of this procedure relies on the electron localization which characterizes many large systems.[39] However, in metallic systems at low-temperature, and for low band semiconductors, the localization length is very large, and such approaches are difficult to apply.[17]

In order to enable treatment of systems in which electron coherence is nonlocal, a different linear scaling approach was proposed and dubbed stochastic density functional theory (sDFT).[40] In sDFT we use a sparse representation of the KS-DM which does not rely on truncation or modification of its elements. Instead, sDFT is based on the paradigm that the expectation values of the system observables can be regarded as random variables in a stochastic process with an expected value and a fluctuation. The fact that estimation of electronic structure quantities can be done by statistical sampling allows for a natural and highly effective implementation of sDFT on parallel architectures.

The source of errors in sDFT is statistical in nature and involves fluctuations, the magnitude of which can be controlled by statistical sampling theory and/or by variance-reducing techniques, such as the embedded-fragment method,[41–44] or the energy windowing approach.[45,

* eran.rabani@berkeley.edu

† roi.baer@huji.ac.il

46] In addition to statistical fluctuations, the sDFT estimates of the electron density and the forces exhibit bias errors resulting from the nonlinear nature of the SCF iterations.[44, 47] The magnitude of the bias can be controlled by using the above-mentioned variance-reducing techniques.

Early implementations of sDFT were based on real-space grid representations of the electron density,[40, 42, 43, 47, 48] and were applied to relatively homogeneous systems: either to pure bulk silicon,[43, 47] silicon with impurities,[46] H-He mixtures,[49] or to finite-sized hydrogen-passivated silicon nanocrystals, and water clusters.[42, 50, 51] We recently demonstrated that the noisy forces produced by sDFT in the real-space grid representation, can be used within a Langevin dynamics approach, to determine structural properties of such large systems. [42, 52]

The real-space implementation of sDFT is especially useful as a starting point for post-processing DFT-based methods, such as the stochastic GW for charge excitations,[53, 54] the stochastic time-dependent DFT and Bethe-Salpeter equations for neutral excitations,[55–57] and for conductance calculations in warm dense matter.[49]

If one is only interested in the ground state atomistic structure real-space grid representation could be quite expensive and a more efficient representation may be beneficial. For this purpose, we recently developed an sDFT approach based on non-orthogonal atom-centered basis sets.[44] We found that the Hamiltonian within this compact basis has a much smaller energy range than in the real-space grid, allowing a significant speedup of sDFT calculations.

Despite the fact that sDFT with the non-orthogonal atom-centered basis set is designed to address the structural properties of large systems, up to now, we did not have the capability to estimate the forces on nuclei and therefore focused only on the electronic energy and density of states.[44] In this paper we develop the necessary theory and computational tools for calculating the forces while maintaining the linear-scaling complexity of sDFT. In addition, we analyze the statistical fluctuations and the biases in the forces, using as a benchmark the heterogeneous system of Tryptophan Zipper 2 (Trp-zip2) peptide solvated in water.

The manuscript is organized as follows: In Section II, we introduce our formalism for the stochastic forces calculations. Then, in Section III, we present the benchmark calculations on the Tryptophan Zipper 2 (Trp-zip2) peptide in solution. Finally, we summarize and discuss the results in Section IV.

II. FORCE CALCULATIONS IN STOCHASTIC DENSITY FUNCTIONAL THEORY

In this section we describe the theory of the electronic forces on nuclei within the finite temperature KS-DFT

formalism. We set the notations and describe the basis set representation we use for Kohn-Sham DFT in subsection II A with the combined implementation using real space grids briefly described in subsection II B. Expressions for the forces are given in subsection II C with a detailed derivation given in Appendix A. Finally, in subsections II D-II E we provide the detail behind the stochastic evaluation of the electronic density and any other observables in sDFT (including the forces), and present the statistical errors involved.

A. Setting the stage

The KS Hamiltonian is given by:

$$\hat{h}_{\text{KS}} = \hat{t}_s + \hat{v}_{pp}^{nl} + \hat{v}_{pp}^{loc} + v_{Hxc}[n](\mathbf{r}), \quad (1)$$

where $\hat{t}_s = -\frac{1}{2}\nabla^2$ (we use atomic units throughout the paper) is the electron kinetic energy operator, $\hat{v}_{pp}^{nl} = \sum_{C \in \text{nuclei}} \hat{v}_{pp(C)}^{nl}$, and $\hat{v}_{pp}^{loc} = \sum_{C \in \text{nuclei}} \hat{v}_{pp(C)}^{loc}(\hat{\mathbf{r}} - \mathbf{R}_C)$ are the non-local and local norm-conserving pseudopotential terms in the Kleinman-Bylander form, [58, 59] for nucleus C , at position \mathbf{R}_C . The last potential term, v_{Hxc} , is the Hartree and exchange correlation potential, depending on the electron density, $n(\mathbf{r})$:

$$\begin{aligned} v_{Hxc}[n](\mathbf{r}) &= \frac{\delta \mathcal{E}_{Hxc}[n]}{\delta n(\mathbf{r})} \\ &= \int \frac{n(\mathbf{r}')}{|\mathbf{r} - \mathbf{r}'|} d^3r' + v_{xc}[n](\hat{\mathbf{r}}), \end{aligned} \quad (2)$$

where $\mathcal{E}_{Hxc}[n]$ is the Hartree and exchange-correlation energy functional.

We use a nonorthogonal atom-centered basis set, $\phi_\alpha(\mathbf{r})$, $\alpha = 1, \dots, K$, with an overlap matrix $S_{\alpha\gamma} = \langle \phi_\alpha | \phi_\gamma \rangle$, $\alpha, \gamma = 1, \dots, K$. Within such a basis set approach, the $K \times K$ DM is given as an operator involving a function of HS^{-1} :

$$P = S^{-1} f(HS^{-1}; \beta, \mu) \quad (3)$$

where $H_{\alpha\gamma} = \langle \phi_\alpha | \hat{h}_{\text{KS}} | \phi_\gamma \rangle$ and

$$f(\varepsilon; \beta, \mu) \equiv \frac{1}{1 + e^{\beta(\varepsilon - \mu)}}. \quad (4)$$

is the Fermi-Dirac distribution function. The DM is used to calculate expected values of single-electron observables \hat{o} as:

$$\langle \hat{o} \rangle = 2 \times \text{Tr}[OP], \quad (5)$$

where O is the matrix representing \hat{o} in the basis, with elements:

$$O_{\alpha\gamma} = \langle \phi_\alpha | \hat{o} | \phi_\gamma \rangle, \quad (6)$$

and the factor of 2 accounts for the electron's spin in a closed shell representation. For example, the expectation

value of the density operator $\hat{n}(\mathbf{r})$ is the electron density, given by:

$$n[P](\mathbf{r}) = \langle \delta(\mathbf{r} - \hat{\mathbf{r}}) \rangle = 2 \times \sum_{\alpha\gamma} P_{\alpha\gamma} \phi_{\alpha}(\mathbf{r}) \phi_{\gamma}(\mathbf{r}), \quad (7)$$

The DM in Eq. (3) minimizes the total electronic free-energy:

$$\Omega[P] = \mathcal{E}[P] - \mu \mathcal{N}[P] - (k_B \beta)^{-1} \mathcal{S}_{ent}[P]. \quad (8)$$

Here $\mathcal{E}[P]$ is the electronic internal energy,

$$\begin{aligned} \mathcal{E}[P] = 2 \times \text{Tr} [(T_s + V_{PP}^{nl} + V_{PP}^{loc}) P] \\ + \mathcal{E}_{Hxc}[n[P]] \end{aligned}$$

and the number of electrons is given by

$$\mathcal{N}[P] = 2 \times \text{Tr}[SP].$$

The actual value we use for the chemical potential μ is tuned to enforce $\mathcal{N}[P]$ to be equal to the actual number of electrons in the system (see Ref.44 for detail). Finally $\mathcal{S}_{ent}[P]$ is the entropy of the non-interacting electrons of the KS system, given by:

$$\begin{aligned} \mathcal{S}_{ent}[P] = -2 \times k_B \text{Tr}[SP \ln SP + \\ (1 - SP) \ln (1 - SP)] \end{aligned}$$

Equations (1)-(7) must be solved together, and the resulting solution for the density $n(\mathbf{r})$ and the DM P is called the self-consistent field (SCF) solution to the KS equations. The procedure for reaching SCF solution is iterative: in each iteration, called an SCF cycle, P is calculated from H using Eq. (3), $n(\mathbf{r})$ from P from which $v_{Hxc}[n](\mathbf{r})$ is calculated and a new KS Hamiltonian matrix H is built.

B. Combined real-space grid and basis set implementation

The theory described in the section above uses, in addition to the basis function $\phi_{\alpha}(\mathbf{r})$, also a Cartesian grid (with uniform grid-spacing h) which spans the space occupied by the electron density. The grid is used to evaluate the matrix elements of Eq. (6) of various observables \hat{o} , expressible as operators on the grid:

$$O_{\alpha\gamma} = h^3 \sum_g \phi_{\alpha}(\mathbf{r}_g) [\hat{o} \phi_{\gamma}](\mathbf{r}_g), \quad (9)$$

where \mathbf{r}_g are the grid points (g is a 3D index). Each matrix element of Eq. (9) can be evaluated efficiently[60] while we can also gain by parallel architecture, allowing different cores to independently compute different $\alpha\gamma$ pairs. In particular, the pseudopotentials $\hat{v}_{PP}^{nl/loc}$ are such grid operators. Evaluating the electron density of Eq. (7) at the grid points allows calculation of the density-dependent Hartree and XC potentials. For the former, we use fast Fourier transform techniques.[61]

C. Electronic forces on the nuclei

In this subsection we give formal expressions for the electronic forces on the nuclei expressible as matrix trace operations, based on a finite temperature formalism presented in Appendix A. Our derivation and final results are similar yet differ in many ways with those of Ref.62. We calculate the work done by the electrons as nucleus C is displaced by $\delta_C X$ in the x -coordinate. This work is the change in the free energy of Eq. (8), and therefore

$$-F_C \delta_C X = \delta_C \Omega \quad (10)$$

where F_C , is the x -component of the force on the displaced nucleus. The atom displacement $\delta_C X$ has three types of effects: it causes an explicit change in its contribution to the pseudopotential $\hat{v}_{pp}^{nl/loc} \rightarrow \hat{v}_{pp}^{nl/loc} + \delta_C \hat{v}_{pp}^{nl/loc}$, it displaces the basis functions $\phi_{\alpha} \rightarrow \phi_{\alpha} + \delta_C \phi_{\alpha}$, and it induces a variation in the DM, $P \rightarrow P + \delta_C P$, since P is required to be the minimizer of the free energy. Note that due to this minimum principle $\delta_C \Omega$ is unaffected (to first order) by $\delta_C P$ so that the work done on the atom (see Appendix A),

$$-F_C \delta_C X = 2 \times \text{Tr}[P(\delta_C H - (HS^{-1})\delta_C S)], \quad (11)$$

is given solely in terms of the variations in the Hamiltonian,

$$\begin{aligned} (\delta_C H)_{\alpha\beta} = \langle \phi_{\alpha} | \delta_C (\hat{v}_{pp}^{nl} + \hat{v}_{pp}^{loc}) | \phi_{\beta} \rangle \\ + \langle \delta_C \phi_{\alpha} | \hat{h}_{KS} | \phi_{\beta} \rangle + \langle \phi_{\alpha} | \hat{h}_{KS} | \delta_C \phi_{\beta} \rangle \end{aligned} \quad (12)$$

and the overlap,

$$(\delta_C S)_{\alpha\beta} = \langle \delta_C \phi_{\alpha} | \phi_{\beta} \rangle + \langle \phi_{\alpha} | \delta_C \phi_{\beta} \rangle \quad (13)$$

matrices. The first term in Eq. (12) is the explicit change in the pseudopotential, giving the direct forces on the atom. The second and third terms in $\delta_C H$ (and similar terms in Eq. (13) for $\delta_C S$) are due to the variation in basis functions, and they lead to the so-called Pulay forces,[63] on the atom. More details concerning the calculation of $(\delta_C S)_{\alpha\beta}$ and $(\delta_C H)_{\alpha\beta}$ are given in the Supporting Information, Section S1.

The estimation of the expectation value of a one-body observable \hat{o} , given by Eq. (5), requires the calculation of the trace of the matrix OP . By definition $\text{Tr}[OP] = \sum_{k=1}^K (u^k)^T OP u^k$ where u^k are a set of K orthogonal unit vectors and the numerical effort involves K applications of OP on a vector u , each of which scales quadratically and thus the overall effort scales as $O(K^3)$.

One essential component in reducing the scaling of this step is to exploit the sparsity of the $S^{-1}H$ operation on a vector v [64], which is used within a Chebyshev expansion,[65] as a Fermi-Dirac function representing P (see Eq. (3)). This leads to the following method for applying the DM onto a vector v [8, 66]:

$$Pv = \sum_{n=0}^{N_C} a_n(\beta, \mu) v_n, \quad (14)$$

where v_n , $n = 0, 1, \dots$ is obtained recursively

$$\begin{aligned} v_0 &= v \\ v_1 &= \left[\frac{HS^{-1} - \bar{E}}{\Delta E} \right] v_0 \\ v_{n+1} &= 2 \left[\frac{HS^{-1} - \bar{E}}{\Delta E} \right] v_n - v_{n-1}. \end{aligned} \quad (15)$$

Here $\frac{HS^{-1} - \bar{E}}{\Delta E}$ is a shifted-scaled operator with eigenvalues in the interval $[-1, 1]$ (so ΔE is equal to half the spectral range and \bar{E} is its center). The expansion coefficients depend on β and μ characterizing the Fermi-Dirac function; they rapidly decay to zero once N_C exceeds a system size independent value determined by $\beta\Delta E$. With this technique, the step Pu^k involves a linear scaling effort, and since there are K such vectors the complexity of the trace operation $\text{Tr}[OP]$ is reduced from $O(K^3)$ to $O(K^2)$. [67]

D. Stochastic estimation of observables and forces

In order to further reduce the numerical effort to linear scaling, we use a stochastic vector approach, where the trace is sampled using I stochastic vectors instead of *calculated* using a complete set of K orthonormal vectors. The calculation effort is reduced from $O(K^2)$ to $O(IK)$ and I is system independent. A full exposition of the method is given in Ref. 44, here we briefly mention the essential elements.

Stochastic vectors $\chi^T = (\chi^1, \dots, \chi^K)$, have K random components, χ^k , each is a random variable taking the values ± 1 with equal probability. We refer the reader to Section S2. of the Supporting Information for definition and discussion of random variables (collectively denoted r) their expected values $E[r]$, their variance $\text{Var}[r]$, and the statistical methods for evaluating these quantities using finite samples. For each component of the stochastic vector: (1) $|\chi^k| = 1$ (2) $E[\chi^k] = 0$ and therefore $\text{Var}[\chi^k] = 1$. Furthermore, the product $\chi^k \chi^j$ of any pair of components has a zero expected value ($E[\chi^k \chi^j] = 0$, $k \neq j$) and hence, in matrix form

$$E[\chi\chi^T] = \text{Id} \quad (16)$$

where Id is the $K \times K$ identity matrix. We view Eq. (16) as the “stochastic resolution of the identity” and using it we express the trace of the matrix OP as $\text{Tr}[OP] = \text{Tr}[OPE[\chi\chi^T]] = E[\text{Tr}[OP\chi\chi^T]]$, which upon rearrangement gives the stochastic trace formula: [68]

$$\langle \hat{o} \rangle = 2 \times E[\chi^T OP \chi]. \quad (17)$$

The expected value $E[\chi^T OP \chi]$ can be estimated using a sample of size I with

$$m_I = 2 \times \frac{1}{I} \sum_{i=1}^I \chi_i^T OP \chi_i \quad (18)$$

which establishes a 70% confidence interval $[m_I - \sigma_I, m_I + \sigma_I]$ for $\langle \hat{o} \rangle$ where

$$\sigma_I = \frac{s_I}{\sqrt{I}} \quad (19)$$

and $s_I = \sqrt{\frac{1}{I-1} \sum_{i=1}^I (\chi_i^T OP \chi_i - m_I)^2}$ is the standard deviation. We would like to highlight that since Eq. (18) is an average over i independent $\chi_i^T OP \chi_i$ terms, the computation is easily implemented to gain from parallel architecture.

We can use the stochastic trace to estimate the electron density at each grid point, based on Eq. (7). For this, we define stochastic orbitals which are stochastic linear combinations of the basis functions, defined on the grid as

$$\eta_i(\mathbf{r}_g) = \sum_{\alpha=1}^K \chi_i^\alpha \phi_\alpha(\mathbf{r}_g)$$

and *projected* stochastic orbitals

$$\xi_i(\mathbf{r}_g) = \sum_{\alpha=1}^K [P\chi_i]^\alpha \phi_\alpha(\mathbf{r}_g).$$

Using the above we can now calculate the center of the confidence interval for the electron density at point \mathbf{r}_g as the sample mean:

$$n_I(\mathbf{r}_g) = 2 \times \frac{1}{I} \sum_{i=1}^I \eta_i(\mathbf{r}_g) \xi_i(\mathbf{r}_g). \quad (20)$$

In Ref. 44 we have presented CPU times showing linear scaling in the calculation of sDFT observables.

The above technique can be used to evaluate the electronic forces on the nuclei as they too are formulated as matrix traces (see Eq. (11)). The computational effort for evaluating the direct forces coming from \hat{v}_{pp}^{nl} (the non-local pseudopotential) as well as all Pulay terms, for each degree of freedom, are independent of the system size since they are local (See Supporting Information Section S1.C. for detail). The computational effort for evaluating the force coming from \hat{v}_{pp}^{loc} (the local pseudopotential), for each degree of freedom, will scale linearly unless specialized particle mesh methods (beyond the scope of this paper) are used.

The SCF cycle of KS theory in sDFT involves using our best estimate for the density, i.e. $n_I(\mathbf{r})$ to build the Hamiltonian. Since $n_I(\mathbf{r})$ includes an uncertainty (a fluctuation), the resulting Hamiltonian matrix H also has a fluctuation. Then, plugging H into the Chebyshev expansion from which a new $n_I(\mathbf{r})$ is calculated converts the fluctuation into a bias, as discussed Section S2.C. of the Supporting Information. Thus after the SCF converges all expectation values have both an uncertainty σ_I and a bias error, which we define as:

$$\Delta\rho_I = \left| E[m_I] - \langle \hat{o} \rangle^{dDFT} \right|.$$

The estimation of the uncertainty σ_I can be done using Eq. (19), but the estimation of $\Delta\rho_I$ is more complicated since we need to determine $E[m_I]$. We discuss this issue when we determine the bias error in the force (see Section III).

E. Embedded fragments approach

In order to mitigate the fluctuation and bias errors we developed a basis set version of the embedded-fragment (EF) approach,[41–44] which can be described in a general way as introducing a correction term to the sDFT calculation. We first split all the atoms in the system into F fragments, such that each atom, and all basis functions centered on it, belong to one and only one fragment. If the fragments are chosen such that their size is independent of the total system size, with sub-linear scaling and minimal increase in computation time we can calculate the electron density in each fragment, using: 1.) deterministic DFT $n_{\text{dDFT}}^f(\mathbf{r})$ ($f = 1, \dots, F$) and 2.) stochastic DFT $n_I^f(\mathbf{r})$. We then use the difference

$$\Delta n^f(\mathbf{r}) = n_{\text{dDFT}}^f(\mathbf{r}) - n_I^f(\mathbf{r}) \quad (21)$$

as a correction to the sDFT calculation of the density $n_I(\mathbf{r})$ on the entire system:

$$n_I^{EF}(\mathbf{r}) = n_I(\mathbf{r}) + \sum_{f=1}^F \Delta n^f(\mathbf{r}). \quad (22)$$

We note, that the correct result, $n_I^{EF}(\mathbf{r}) = n_{\text{dDFT}}(\mathbf{r})$ is obtained in two limits: 1) when $F = 1$ (i.e. the entire system is a fragment) and 2) when $I \rightarrow \infty$, so $n_I^f(\mathbf{r}) \rightarrow n_{\text{dDFT}}^f(\mathbf{r})$ etc. Similarly, the expectation value of any operator of interest, \hat{o} :

$$\langle \hat{o} \rangle_I^{EF} = \langle \hat{o} \rangle_I + \sum_f \langle \Delta \hat{o}^f \rangle_I \quad (23)$$

where $\langle \Delta \hat{o}^f \rangle_I = \langle \hat{o}^f \rangle_{\text{dDFT}} - \langle \hat{o}^f \rangle_I$. The EF approach is applicable to the forces calculation, by choosing \hat{o} to be the relevant operators from Eq. (11). For further detail on the implementation of the embedded fragments method in our program, see Supporting Information, Section S3.

III. STATISTICAL ANALYSIS OF SDFT FORCES IN THE TRYPTOPHAN ZIPPER 2 PEPTIDE

Our test system is a Tryptophan Zipper 2 (Trp-zip2) peptide (pdb 1le1), composed of 220 atoms (left panel of Fig. 1), solvated with 425 water molecules and built using a universal force field (UFF) in ArgusLab,[69, 70] (right panel of Fig. 1). For benchmark calculations we

focused on the 20 nitrogen atoms of the peptide (indexed by C) and calculated the forces acting on each Cartesian degree of freedom. In these calculations, the embedded-fragment method was used, for which we chose to consider the peptide as a single fragment and then divided the 425 water molecules into 27 fragments, with an average size of 16 molecules.

To study the statistical errors we performed the sDFT calculations using increasing number of stochastic vectors, $I = 12, 120, 1200$, according to Eq. (17). To estimate the magnitudes of the bias and the uncertainty we repeated the calculations M times (using independent random number generator seeds) from which we calculated a sample average force vector:

$$\bar{\mathbf{F}}_C = \frac{1}{M} \sum_{m=1}^M \mathbf{F}_C^m,$$

and a 3×3 force covariance matrix:

$$\Sigma^2 = \frac{1}{M} \sum_{m=1}^M (\mathbf{F}_C^m - \bar{\mathbf{F}}_C) (\mathbf{F}_C^m - \bar{\mathbf{F}}_C)^T,$$

as an estimate for the covariance of the sDFT calculation. As the forces acting on each atom are represented as a 3-dimensional vectors (over the Cartesian coordinates) we would like to obtain scalar values, irrespective of the way the Cartesian axes are defined, in order to estimate the uncertainty and bias of the sDFT forces[71]. For a canonical estimate of the uncertainty we use an average over the eigenstates of Σ^2 :

$$\sigma_C = \sqrt{\frac{1}{3} \text{Tr} \Sigma^2}, \quad (24)$$

where $F_C^{dDFT} = \|\mathbf{F}_C^{dDFT}\|$, is the magnitude of the dDFT electronic force on atom C . For a canonical estimate of the bias in the force we use the L_2 -Norm of the error in the average force vector:

$$\Delta\rho_C = \|\bar{\mathbf{F}}_C - \mathbf{F}_C^{dDFT}\|. \quad (25)$$

In Fig. 2 we present data for the statistical errors in the forces of the 20 Nitrogen atoms, ordered by an atom index according to their distance from the center of the peptide (1 closest, 20 furthest). The estimates for the uncertainty in the forces, σ_C of Eq. (24) are plotted in blue circles, while the estimates of the bias $\Delta\rho_C$ of Eq. (25), with an error bar calculated as $\pm\sigma_C/\sqrt{M}$, in orange triangles with blue error bars. The medians over all Nitrogen atoms are plotted as dashed lines. The used number of stochastic vectors, I , as well as the number of repetitions, M , is shown above each panel. We found that stable estimates of σ_C are obtained even when using a small number of $M \approx 50$ repetitions and observe that they obey the expected $1/\sqrt{I}$ behavior in accordance with the central limit theorem. Since the variance is given by the

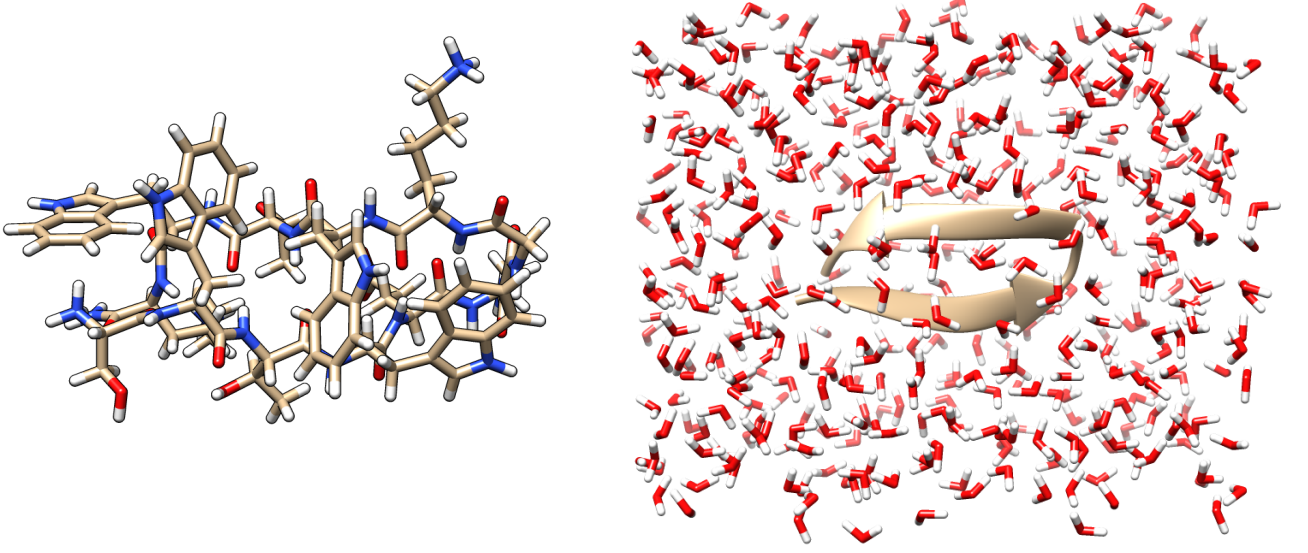


Figure 1. Left Panel: Tryptophan Zipper 2 (Trp-zip2) peptide, composed of 220 atoms. Right Panel: Trp-zip2 peptide (ribbon) solvated by 425 water molecules. The full system is composed of 1495 atoms, 4024 valence electrons and 3118 basis functions are necessary to describe it using a minimal basis set.

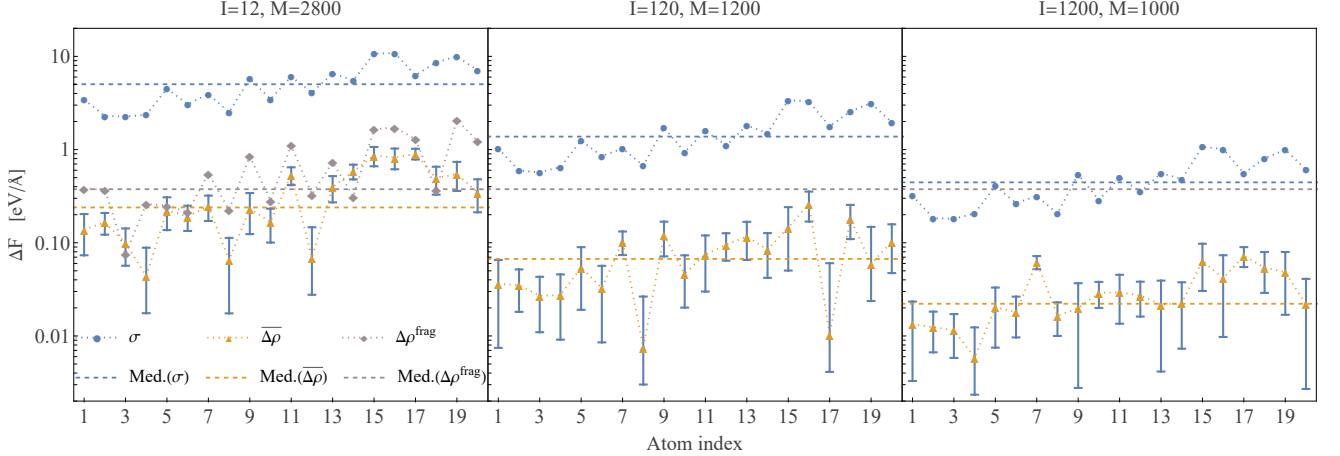


Figure 2. The statistical errors in the sDFT forces acting on the 20 nitrogen atoms in the solvated-TrpZip2 system calculated using $I = 12, 120, 1200$ stochastic vectors (see left, center and right panels). For each Nitrogen atom, we show the uncertainty σ_C (blue dots), and the estimate in the bias $\Delta\rho_C$ (orange triangles), see Eqs. 24,25 in text, with error bars calculated as $\pm\sigma_C/\sqrt{M}$. In the $I = 12$ column we also plot $\Delta\rho_C^{frag} = \|\mathbf{F}_C^{frag} - \mathbf{F}_C^{dDFT}\|$ (gray diamonds), where \mathbf{F}_C^{frag} is the dDFT force vector on the Nitrogen atom C from the peptide-only fragment calculation. The dotted lines connecting the markers are presented as a guide for the eye, while the dashed horizontal lines are medians over all atoms of σ_C and $\Delta\rho_C$. For simplification of the image, in the $I = 120, 1200$ columns we only present the median of $\Delta\rho_C^{frag}$ (gray dashed line) taken over all 20 Nitrogen atoms.

matrix elements of the system, (see Supporting Information, Section S2.C, Eq. (S3)), the pattern seen for σ_C as a function of atom index is almost unchanged for different values of I . To estimate the bias we need a good estimate of $E[m_I]$ (the expected value of the forces when calculated using I stochastic vectors in Eq. (18)). As σ_C is much larger than $\Delta\rho_C$, a very large number of repetitions, M , was required in order to achieve a good enough

estimate of $E[m_I]$ such that $\Delta\rho_C$ values are useful estimates of the bias. It is clear from the error bars that for almost all Nitrogen atoms we have good estimates of the bias.

In the $I = 12$ column, for an added perspective, we plot in gray diamonds, the error $\Delta\rho_C^{frag} = \|\mathbf{F}_C^{frag} - \mathbf{F}_C^{dDFT}\|$, where \mathbf{F}_C^{frag} is the force vector on

the Nitrogen atom C from a dDFT calculation on its peptide only (gas-phase) fragment. The median is given again, in a dashed line. We observe that the values of $\Delta\rho_C^{frag}$ for the atoms closer to the center of the fragment are mostly smaller than those further away, causing a similar pattern in the sDFT errors. When comparing the median of $\Delta\rho_C^{frag}$ (plotted for all panels in a gray dashed line) with those of the stochastic results, we see they are higher even for the $I = 12$ stochastic vectors case, whereas for the cases of $I = 120, 1200$ we observe a reduction in the errors, showing that overall sDFT significantly improves the force estimation in comparison to the deterministic fragment calculation[72].

Additional sDFT calculations on a smaller system, composed of the Trp-zip2 peptide and only 195 solvating water molecules, show that for a given number of stochastic orbitals ($I = 12$) the uncertainty and bias are very similar to the case of the original solvated system (see Supporting Information, Section S4.) . This suggests the statistical errors are roughly independent of system size.

IV. SUMMARY AND CONCLUSIONS

We have presented a method for force calculations within finite temperature sDFT in nonorthogonal atom-centered basis sets. The forces are random variables evaluated using the stochastic trace formula applied to various operators derived from the free energy, and are therefore, like all sDFT observables, characterized by statistical errors, a fluctuation and a bias. The calculation of the forces is adapted to benefit from the embedded-fragment methodology. These calculations are dominated by the SCF sDFT convergence step and therefore the times for force calculations are similar to those reported in Ref.44.

In Section III we presented benchmarking calculations, focusing on the statistical errors in the force estimates for the 20 Nitrogen atoms of a solvated Tryptophan Zipper 2 peptide system. The results are given as a function of I , the number of stochastic vectors used in the calculation according to Eq. (17). The uncertainty in the sDFT forces follows the expected $1/\sqrt{I}$ behavior in accordance with the central limit theorem. Using a very large number of repetitions we were also able to uncover the bias and determine that it is at least an order of magnitude smaller than the uncertainty. The magnitude of the force bias is of the order of 0.065 eV/\AA ($\sim 10^{-3} E_h/a_0$) when 120 stochastic orbitals are used, independently of system size. A back-of-the-envelope calculation shows that this magnitude of bias is sufficiently small to ensure that the bond lengths estimated by stochastic DFT (within a Langevin molecular dynamics simulation) will deviate by less than 1% from those predicted by a deterministic calculation[73]. Indeed, this fact was demonstrated using a Langevin Dynamics simulation on silicon nanocrystals,[42] within a real-space representation sDFT. Our present results indicate that sDFT based on

nonorthogonal atom-centered basis sets can be also used successfully in this way.

It is instructive to discuss the efficiency and accuracy of the basis set[44] vs. real-space grid[40, 42] representations of sDFT calculations. For this, we used the $\text{Si}_{35}\text{H}_{36}$ system, comparing the 6-31G basis set calculations with those of a real-space grid having 64^3 points and grid-spacing of $\delta x = 0.5a_0$ (for more information about this comparison see the Supporting Information, Section S5.). We find that the time for application of the density matrix to a random vector in the 6-31G basis is a factor 30 faster than in the grid representation. On the other hand, surprisingly, the standard deviation of fluctuations in a typical Si force component is about 5 times larger in the basis set calculation than in the grid. Therefore, we need a factor of $5^2 = 25$ more stochastic vectors (because their number is proportional to the square of the standard deviation) in the basis set calculation for achieving the same fluctuation error. If we had only a single processor, the two representations would thus require a similar numerical effort for achieving a given fluctuation goal: the grid is 30 times slower but requires a factor of 25 less samplings. Due to the highly parallelizable nature of sDFT, the necessary extra sampling required by the basis-set-based calculation, does not automatically lead to increased wall-times, if additional CPUs can be offered. We conclude that the basis-set-based calculations can achieve smaller wall-times than real-space grids, given additional CPUs.

ACKNOWLEDGMENTS

RB and ER gratefully thank the Binational Science Foundation grant No. 2018368. ER acknowledges support from the Center for Computational Study of Excited State Phenomena in Energy Materials (C2SEPME) at the Lawrence Berkeley National Laboratory, which is funded by the U.S. Department of Energy, Office of Science, Basic Energy Sciences, Materials Sciences and Engineering Division under Contract No. DE-AC02-05CH11231 as part of the Computational Materials Sciences Program.

SUPPORTING INFORMATION AVAILABLE

Evaluation of the force matrix elements (Section S1.), basic concepts in statistics (Section S2.), the embedded fragment method (Section S3.), system size dependency of statistical errors (Section S4.), efficiency of representations (Section S5.). This information is located after the references.

Appendix A: Derivation of the changes in free energy

Here, we derive the force expression of Eq. (11). The force is given by the change in free energy

$$\Omega[P] = \mathcal{E}[P] - \mu \mathcal{N}[P] - (k_B \beta)^{-1} \mathcal{S}_{ent}[P]$$

due to displacement of the nuclei. When nuclei are displaced the DM also changes, we will show that under any change in the density matrix $P \rightarrow P + \delta_0 P$, while keeping the nuclei fixed, the free energy of Eq. (8) does not change when P is given by Eq. (3). This will be done by examining each term in the above equation separately and summing over all of them. Then we will consider the direct change in free energy due to a displacement of the nuclei (while P is held constant). It is only this latter change which affects the free energy.

1. The variation in $\mathcal{N}[P]$

Starting from:

$$\mathcal{N}[P] = \int n[P](\mathbf{r}) d\mathbf{r}$$

and

$$n[P](\mathbf{r}) = 2 \times \sum_{\alpha\gamma} P_{\alpha\gamma} \phi_\alpha(\mathbf{r}) \phi_\gamma(\mathbf{r}).$$

Combining these we see

$$\mathcal{N}[P] = 2 \times \text{Tr}[SP].$$

We consider two types of variations: δ_0 which change the DM but not the atoms and δ_C which change the position of atom C (and thus affects the basis functions associated with that atom) but not P .

1. $P \rightarrow P + \delta_0 P$ (assuming nuclei are constant): Here

$$\delta_0 n(\mathbf{r}) = 2 \times \sum_{\alpha\gamma} \delta_0 P_{\alpha\gamma} \phi_\alpha(\mathbf{r}) \phi_\gamma(\mathbf{r}) \quad (\text{A1})$$

so

$$\delta_0 \mathcal{N}[P] = 2 \times \text{Tr}[S \delta_0 P] \quad (\text{A2})$$

2. Nucleus C moves by $\delta_C X$ (and $\phi_\alpha \rightarrow \phi_\alpha + \delta_C \phi_\alpha$) (constraining P to be constant): the change in the density is

$$\begin{aligned} \delta_C n(\mathbf{r}) = 2 \times \sum_{\alpha\gamma} P_{\alpha\gamma} [\delta_C \phi_\alpha(\mathbf{r}) \phi_\gamma(\mathbf{r}) \\ + \phi_\alpha(\mathbf{r}) \delta_C \phi_\gamma(\mathbf{r})]. \end{aligned}$$

so:

$$\delta_C \mathcal{N}[P] = 2 \times \text{Tr}[P \delta_C S] \quad (\text{A3})$$

using the change in the overlap matrix

$$(\delta_C S)_{\alpha\beta} = \langle \delta_C \phi_\alpha | \phi_\beta \rangle + \langle \phi_\alpha | \delta_C \phi_\beta \rangle \quad (\text{A4})$$

2. The variation in $\mathcal{E}[P]$

Starting from:

$$\mathcal{E}[P] = 2 \times \text{Tr}[(T_s + V_{PP}^{nl} + V_{PP}^{loc})P] + \mathcal{E}_{Hxc}[n[P]]$$

we have two types of variations, δ_0 which change the DM but not the atoms and δ_C which change the position of atom C (and thus affects the basis functions associated with that atom) but not P .

1. $P \rightarrow P + \delta_0 P$ (freezing the nuclei). We have that

$$\delta_0 \mathcal{E}_{Hxc}[n[P]] = \int v_{Hxc}(n[P](\mathbf{r})) \delta_0 n(\mathbf{r}) d\mathbf{r}$$

so using Eq. (A1)

$$\delta_0 \mathcal{E}[P] = 2 \times \text{Tr}[H \delta_0 P] \quad (\text{A5})$$

2. Nucleus C moves by $\delta_C X$ (and $\phi_\alpha \rightarrow \phi_\alpha + \delta_C \phi_\alpha$) (constraining P to be constant): we find

$$\delta_C \mathcal{E}[P] = 2 \times \text{Tr}[P \delta_C H] \quad (\text{A6})$$

where

$$\begin{aligned} (\delta_C H)_{\alpha\beta} = \langle \phi_\alpha | \delta_C (\hat{v}_{pp}^{nl} + \hat{v}_{pp}^{loc}) | \phi_\beta \rangle \\ + \langle \delta_C \phi_\alpha | \hat{h}_{KS} | \phi_\beta \rangle + \langle \phi_\alpha | \hat{h}_{KS} | \delta_C \phi_\beta \rangle \end{aligned} \quad (\text{A7})$$

3. The variation in $\mathcal{S}_{ent}[P]$

Starting from $\mathcal{S}_{ent}[P] = -2 \times k_B \text{Tr}[SP \ln(SP) + (1 - SP) \ln(1 - SP)]$,

1. $P \rightarrow P + \delta_0 P$ (freezing the nuclei) We have by derivation that

$$\begin{aligned} \delta_0 \mathcal{S}_{ent}[n[P]] \\ = -2 \times k_B \text{Tr} \left[\ln \left(\frac{SP}{1 - SP} \right) S \delta_0 P \right] \end{aligned} \quad (\text{A8})$$

2. Nucleus C moves by $\delta_C X$ (and $\phi_\alpha \rightarrow \phi_\alpha + \delta_C \phi_\alpha$) (constraining P to be constant), we find:

$$\delta_C \mathcal{S}_{ent}[n[P]] = -2 \times k_B \text{Tr} \left[\ln \left(\frac{SP}{1 - SP} \right) P \delta_C S \right] \quad (\text{A9})$$

4. The variation in $\Omega[P]$

Here we combine the above results, while using the relationship:

$$\left(\mu - \beta^{-1} \ln \frac{SP}{1 - SP} \right) = H S^{-1},$$

which we find by substituting in Eq. (3) for P .

1. $P \rightarrow P + \delta_0 P$ (freezing the nuclei) Using Eqs. (A2), (A5) and (A8), we have

$$\delta_0 \Omega = 2 \times \text{Tr} \left[\left\{ H - \left(\mu - \beta^{-1} \ln \frac{SP}{1-SP} \right) S \right\} \delta_0 P \right]$$

leading to

$$\delta_0 \Omega = 0.$$

This reflects the fact that P of Eq. (3) minimizes $\Omega[P]$.

2. Nucleus C moves by $\delta_C X$ (and $\phi_\alpha \rightarrow \phi_\alpha + \delta_C \phi_\alpha$) (since a variation in P does not affect the value of

Ω we can take it as a constant): using Eqs. (A3), (A6) and (A9), we find

$$\delta_C \Omega = 2 \times \text{Tr} [P (\delta_C H - H S^{-1} \delta_C S)]. \quad (\text{A10})$$

The change in free energy is composed of two terms: a term due to the energy, $\delta_C H$ (which includes a direct change and a Pulay term, see Eq. (A7)), and a change due to entropy, which depends purely on Pulay changes in the overlap matrix, $\delta_C S$ (see (A4)).

-
- [1] D. Marx and J. Hutter, *Ab Initio Molecular Dynamics: Basic Theory and Advanced Methods* (Cambridge University Press, 2009) google-Books-ID: VRZUw8Wk4CIC.
 - [2] D. C. Rapaport, *The Art of Molecular Dynamics Simulation* (Cambridge University Press, 2004) google-Books-ID: iqDJ2hjQBMEC.
 - [3] F. Graziani, M. P. Desjarlais, R. Redmer, and S. B. Trickey, *Frontiers and Challenges in Warm Dense Matter*, Vol. 96 (Springer Science & Business, 2014).
 - [4] D. J. Huggins, P. C. Biggin, M. A. Damgen, J. W. Essex, S. A. Harris, R. H. Henchman, S. Khalid, A. Kuzmanic, C. A. Laughton, J. Michel, A. J. Mulholland, E. Rosta, M. S. P. Sansom, and M. W. van der Kamp, *WIREs Comput Mol Sci* **9**, e1393 (2019).
 - [5] W. T. Yang, *Phys. Rev. Lett.* **66**, 1438 (1991).
 - [6] X. Li, W. Nunes, and D. Vanderbilt, *Phys. Rev. B* **47**, 10891 (1993).
 - [7] P. Ordejon, D. A. Drabold, M. P. Grumbach, and R. M. Martin, *Physical Review B-Condensed Matter* **48**, 14646 (1993).
 - [8] S. Goedecker and L. Colombo, *Phys. Rev. Lett.* **73**, 122 (1994).
 - [9] R. W. Nunes and D. Vanderbilt, *Physical Review B-Condensed Matter* **50**, 17611 (1994).
 - [10] Y. Wang, G. M. Stocks, W. A. Shelton, D. M. C. Nicholson, Z. Szotek, and W. M. Temmerman, *Phys. Rev. Lett.* **75**, 2867 (1995).
 - [11] E. Hernandez and M. J. Gillan, *Physical Review B-Condensed Matter* **51**, 10157 (1995).
 - [12] S. Goedecker, *Journal of Computational Physics* **118**, 261 (1995).
 - [13] P. Ordejon, E. Artacho, and J. M. Soler, *Physical Review B-Condensed Matter* **53**, 10441 (1996).
 - [14] D. R. Bowler, M. Aoki, C. M. Goringe, A. P. Horsfield, and D. G. Pettifor, *Modell. Simul. Mater. Sci. Eng.* **5**, 199 (1997).
 - [15] R. Baer and M. Head-Gordon, *The Journal of Chemical Physics* **107**, 10003 (1997).
 - [16] A. H. R. Palser and D. E. Manolopoulos, *Physical Review B-Condensed Matter* **58**, 12704 (1998).
 - [17] S. Goedecker, *Rev. Mod. Phys.* **71**, 1085 (1999).
 - [18] G. E. Scuseria, *The Journal of Physical Chemistry A* **103**, 4782 (1999), publisher: ACS Publications.
 - [19] G. Galli, *Physica Status Solidi B-Basic Research* **217**, 231 (2000).
 - [20] S. Adhikari and R. Baer, *The Journal of Chemical Physics* **115**, 11 (2001).
 - [21] J. M. Soler, E. Artacho, J. D. Gale, A. Garcia, J. Junquera, P. Ordejon, and D. Sanchez-Portal, *J. Phys. C* **14**, 2745 (2002).
 - [22] C. K. Skylaris, P. D. Haynes, A. A. Mostofi, and M. C. Payne, *J. Phys. C* **17**, 5757 (2005).
 - [23] M. J. Gillan, D. R. Bowler, A. S. Torralba, and T. Miyazaki, *Comput. Phys. Commun.* **177**, 14 (2007).
 - [24] C. Ochsenfeld, J. Kussmann, and D. S. Lambrecht, in *Reviews in Computational Chemistry* (Wiley-Blackwell, 2007) pp. 1–82.
 - [25] V. Havu, V. Blum, P. Havu, and M. Scheffler, *Journal of Computational Physics* **228**, 8367 (2009).
 - [26] L. Lin, J. Lu, L. Ying, and E. Weinan, *Chinese Annals of Mathematics, Series B* **30**, 729 (2009).
 - [27] T. Ozaki, *Phys. Rev. B* **82**, 075131 (2010).
 - [28] D. Bowler and T. Miyazaki, *Rep. Prog. Phys.* **75**, 036503 (2012).
 - [29] J. E. Moussa, *J. Chem. Phys.* **145**, 164108 (2016).
 - [30] L. E. Ratcliff, S. Mohr, G. Huhs, T. Deutsch, M. Masella, and L. Genovese, *WIREs Comput Mol Sci* **7**, e1290 (2017).
 - [31] T. D. Kuhne, M. Iannuzzi, M. Del Ben, V. V. Rybkin, P. Seewald, F. Stein, T. Laino, R. Z. Khalullin, O. Schutt, F. Schiffrmann, D. Golze, J. Wilhelm, S. Chulkov, M. H. Bani-Hashemian, V. Weber, U. Borstnik, M. Taillefumier, A. S. Jakobovits, A. Lazzaro, H. Pabst, T. Muller, R. Schade, M. Guidon, S. Andermatt, N. Holmberg, G. K. Schenter, A. Hehn, A. Bussy, F. Belleflamme, G. Tabacchi, A. Glock, M. Lass, I. Bethune, C. J. Mundy, C. Plessl, M. Watkins, J. VandeVondele, M. Krack, and J. Hutter, *J. Chem. Phys.* **152**, 194103 (2020).
 - [32] J. C. A. Prentice, J. Aarons, J. C. Womack, A. E. A. Allen, L. Andrinopoulos, L. Anton, R. A. Bell, A. Bhandari, G. A. Bramley, R. J. Charlton, R. J. Clements, D. J. Cole, G. Constantinescu, F. Corsetti, S. M.-M. Dubois, K. K. B. Duff, J. M. Escartin, A. Greco, Q. Hill, L. P. Lee, E. Linscott, D. D. O'Regan, M. J. S. Phipps, L. E. Ratcliff, A. R. Serrano, E. W. Tait, G. Teobaldi, V. Vitale,

- N. Yeung, T. J. Zuehlsdorff, J. Dziedzic, P. D. Haynes, N. D. M. Hine, A. A. Mostofi, M. C. Payne, and C.-K. Skylaris, *J. Chem. Phys.* **152**, 174111 (2020).
- [33] A. Nakata, J. S. Baker, S. Y. Mujahed, J. T. L. Poulton, S. Arapan, J. Lin, Z. Raza, S. Yadav, L. Truflandier, T. Miyazaki, and D. R. Bowler, *J. Chem. Phys.* **152**, 164112 (2020).
- [34] B. Hourahine, B. Aradi, V. Blum, F. Bonafé, A. Bucchini, C. Camacho, C. Cevallos, M. Y. Deshayé, T. Dumitrică, A. Dominguez, S. Ehlert, M. Elstner, T. van der Heide, J. Hermann, S. Irle, J. J. Kranz, C. Köhler, T. Kowalczyk, T. Kubař, I. S. Lee, V. Lutsker, R. J. Maurer, S. K. Min, I. Mitchell, C. Negre, T. A. Niehaus, A. M. N. Niklasson, A. J. Page, A. Pecchia, G. Penazzi, M. P. Persson, J. Rezáč, C. G. Sánchez, M. Sternberg, M. Stöhr, F. Stuckenberg, A. Tkatchenko, V. W.-z. Yu, and T. Frauenheim, *J. Chem. Phys.* **152**, 124101 (2020).
- [35] B. Aradi, B. Hourahine, and T. Frauenheim, *J. Phys. Chem. A* **111**, 5678 (2007).
- [36] M. Elstner, P. Hobza, T. Frauenheim, S. Suhai, and E. Kaxiras, *The Journal of Chemical Physics* **114**, 5149 (2001).
- [37] W. C. Witt, G. Beatriz, J. M. Dieterich, and E. A. Carter, *J. Mater. Res.* **33**, 777 (2018).
- [38] V. V. Karasiev, T. Sjostrom, and S. B. Trickey, *Computer Physics Communications* **185**, 3240 (2014).
- [39] W. Kohn, *Phys. Rev. Lett.* **76**, 3168 (1996).
- [40] R. Baer, D. Neuhauser, and E. Rabani, *Phys. Rev. Lett.* **111**, 106402 (2013).
- [41] D. Neuhauser, R. Baer, and E. Rabani, *J. Chem. Phys.* **141**, 041102 (2014).
- [42] E. Arnon, E. Rabani, D. Neuhauser, and R. Baer, *The Journal of Chemical Physics* **146**, 224111 (2017).
- [43] M. Chen, R. Baer, D. Neuhauser, and E. Rabani, *J. Chem. Phys.* **150**, 034106 (2019).
- [44] M. D. Fabian, B. Shpiro, E. Rabani, D. Neuhauser, and R. Baer, *Wiley Interdisciplinary Reviews: Computational Molecular Science* **10.1002/wcms.1412**, e1412 (2019).
- [45] M. Chen, R. Baer, D. Neuhauser, and E. Rabani, *J. Chem. Phys.* **151**, 114116 (2019).
- [46] M. Chen, R. Baer, D. Neuhauser, and E. Rabani, *J. Chem. Phys.* **154**, 204108 (2021).
- [47] Y. Cytter, E. Rabani, D. Neuhauser, and R. Baer, *Phys. Rev. B* **97**, 115207 (2018).
- [48] R. Baer and E. Rabani, *The Journal of Chemical Physics* **138**, 051102 (2013).
- [49] Y. Cytter, E. Rabani, D. Neuhauser, M. Preising, R. Redmer, and R. Baer, *Physical Review B* **100** (2019), 10.1103/PhysRevB.100.195101.
- [50] D. Neuhauser, E. Rabani, Y. Cytter, and R. Baer, *J. Phys. Chem. A* **120**, 3071 (2016).
- [51] A. J. Lee, M. Chen, W. Li, D. Neuhauser, R. Baer, and E. Rabani, *Phys. Rev. B* **102**, 035112 (2020).
- [52] E. Arnon, E. Rabani, D. Neuhauser, and R. Baer, *J. Chem. Phys.* **152**, 161103 (2020).
- [53] D. Neuhauser, Y. Gao, C. Arntsen, C. Karshenas, E. Rabani, and R. Baer, *Phys. Rev. Lett.* **113**, 076402 (2014).
- [54] V. Vlček, E. Rabani, D. Neuhauser, and R. Baer, *Journal of Chemical Theory and Computation* **13**, 4997 (2017).
- [55] E. Rabani, R. Baer, and D. Neuhauser, *Phys. Rev. B* **91**, 235302 (2015).
- [56] Y. Gao, D. Neuhauser, R. Baer, and E. Rabani, *J. Chem. Phys.* **142**, 034106 (2015).
- [57] V. Vlček, R. Baer, and D. Neuhauser, *J. Chem. Phys.* **150**, 184118 (2019).
- [58] N. Troullier and J. L. Martins, *Phys. Rev. B* **43**, 1993 (1991).
- [59] L. Kleinman and D. M. Bylander, *Phys. Rev. Lett.* **48**, 1425 (1982).
- [60] This requires a fast evaluation of basis functions $\phi_\alpha(\mathbf{r}_g)$ at the grid points. For this, we employ standard quantum-chemical Cartesian functions, expressible as sums of triple products, $\phi_\alpha(x, y, z) = \sum_p \xi_\alpha^p(x) \eta_\alpha^p(y) \zeta_\alpha^p(z)$ where the sums of $\xi_\alpha^p(x)$, $\eta_\alpha^p(y)$ and $\zeta_\alpha^p(z)$ are the primitive functions of the basis. At grid point \mathbf{r}_g the basis function is a sum (over the primitive functions) of triple products formed from three 1D vectors: $\xi_\alpha^p(x_g)$, $\eta_\alpha^p(y_g)$ and $\zeta_\alpha^p(z_g)$ which are kept in memory. The same technique is used for the evaluation of the derivatives of the basis functions, which is relevant for the calculation of forces, see Supporting Information, Section S1.
- [61] G. J. Martyna and M. E. Tuckerman, *J. Chem. Phys.* **110**, 2810 (1999).
- [62] A. M. Niklasson, *The Journal of chemical physics* **129**, 244107 (2008).
- [63] P. Pulay, *Molecular Physics* **17**, 197 (1969), publisher: Taylor & Francis _eprint: <https://doi.org/10.1080/00268976900100941>.
- [64] The application of S^{-1} on a column vector involves repeated applications of S on the vector, within the preconditioned conjugate gradient method, implemented in the HSL-MA61 code. HSL is a collection of FORTRAN codes for large scale scientific computation (<http://www.hsl.rl.ac.uk/>).
- [65] H. Tal-Ezer and R. Kosloff, *J. Chem. Phys.* **81**, 3967 (1984).
- [66] R. Baer and M. Head-Gordon, *Phys. Rev. Lett.* **79**, 3962 (1997).
- [67] M. Fabian, B. Shpiro, and R. Baer, Submitted (2021).
- [68] M. F. Hutchinson, *Commun Stat Simul Comput.* **19**, 433 (1990).
- [69] M. A. Thompson, Planaria Software LLC, Seattle, WA (2004).
- [70] M. Thompson, in *ACS meeting, Philadelphia*, Vol. 172 (2004) p. 42.
- [71] In addition to the analysis given here, we also present the distribution of the errors $F_C^m - F_C^{dDFT}$ in the Supporting Information, Section S2.D.
- [72] We base this conclusion on the medians of $\Delta\rho_C$. The same conclusions are valid also when considering the largest error, $\max_C \{\Delta\rho_C\}$.
- [73] Assuming the minimum of the Born Oppenheimer potential is harmonic with a local force constant k , the bond length deviation δR due to a force perturbation δF obeys $|k\delta R| = |\delta F|$. In typical solids and molecules k is on the order of 5 to 100 eV/Å⁻² [?] so for δF of the order of 0.065 eV/Å we find $\delta R \lesssim 0.01$ Å, 1% or less for most bond lengths of interest.

Supporting Information: Forces from Stochastic Density Functional Theory under Nonorthogonal Atom-Centered Basis Sets

Ben Shpiro

*Fritz Haber Center for Molecular Dynamics and Institute of Chemistry,
The Hebrew University of Jerusalem, Jerusalem 9190401, Israel*

Marcel David Fabian

*Fritz Haber Center for Molecular Dynamics and Institute of Chemistry,
The Hebrew University of Jerusalem, Jerusalem 9190401, Israel*

Eran Rabani*

*Department of Chemistry, University of California, Berkeley, California 94720, United States
Materials Sciences Division, Lawrence Berkeley National Laboratory, Berkeley, California 94720, United States and
The Raymond and Beverly Sackler Center of Computational Molecular
and Materials Science, Tel Aviv University, Tel Aviv 69978, Israel*

Roi Baer†

*Fritz Haber Center for Molecular Dynamics and Institute of Chemistry,
The Hebrew University of Jerusalem, Jerusalem 9190401, Israel*

I. EVALUATING MATRIX ELEMENTS FOR FORCES

In this section we will describe how to calculate $(\delta_C S)_{\alpha\beta} = \left(\frac{\partial}{\partial X_C} S\right)_{\alpha\beta} \delta_C X$:

$$\left(\frac{\partial}{\partial X_C} S\right)_{\alpha\beta} = \left\langle \frac{\partial}{\partial X_C} \phi_\alpha \middle| \phi_\beta \right\rangle + \left\langle \phi_\alpha \middle| \frac{\partial}{\partial X_C} \phi_\beta \right\rangle$$

and $(\delta_C H)_{\alpha\beta} = \left(\frac{\partial}{\partial X_C} H\right)_{\alpha\beta} \delta_C X$:

$$\begin{aligned} \left(\frac{\partial}{\partial X_C} H\right)_{\alpha\beta} &= \left\langle \phi_\alpha \middle| \frac{\partial}{\partial X_C} \hat{h}_{KS} \middle| \phi_\beta \right\rangle \\ &+ \left\langle \frac{\partial}{\partial X_C} \phi_\alpha \middle| \hat{h}_{KS} \middle| \phi_\beta \right\rangle + \left\langle \phi_\alpha \middle| \hat{h}_{KS} \middle| \frac{\partial}{\partial X_C} \phi_\beta \right\rangle \end{aligned}$$

used in Eq. 11 in the manuscript.

A. The Pulay forces

Here we give the detail of calculating the $\left\langle \frac{\partial}{\partial X_C} \phi_\alpha \middle| \phi_\beta \right\rangle$ and $\left\langle \frac{\partial}{\partial X_C} \phi_\alpha \middle| \hat{h}_{KS} \middle| \phi_\beta \right\rangle$ type matrix elements. For these we need to calculate the derivatives of the basis functions $\phi(\mathbf{r}_g - \mathbf{R}_C)$ with respect to nuclear coordinates $R_C = (X_C, Y_C, Z_C)$. Since we use Cartesian Gaussian functions as our basis we enjoy the ease of calculating their values and derivatives analytically on the grid. Each atom-centered basis function is a sum of primitives, $e^{-\gamma x^2} x^l \times e^{-\gamma y^2} y^m \times e^{-\gamma z^2} z^n$, where $n+l+m$ is the total angular momentum quantum number. Therefore each primitive can be represented by three 1-dimensional vectors $\xi_\alpha(x_g - X_C)$, $\eta_\alpha(y_g - Y_C)$ and $\zeta_\alpha(z_g - Z_C)$ and the function is defined inside a “window” surrounding the atom C and given as a product of three terms at each of its grid points:

$$\phi_\alpha(\mathbf{r}_g) = \xi_\alpha(x_g - X_C) \eta_\alpha(y_g - Y_C) \zeta_\alpha(z_g - Z_C).$$

* eran.rabani@berkeley.edu

† roi.baer@huji.ac.il

The grid is then used to evaluate the matrix elements of the overlap and Hamiltonian matrices:

$$S_{\alpha\beta} = h^3 \sum_{\mathbf{r}_g} \phi_{\alpha}(\mathbf{r}_g) \phi_{\beta}(\mathbf{r}_g),$$

$$H_{\alpha\beta} = h^3 \sum_{\mathbf{r}_g} \phi_{\alpha}(\mathbf{r}_g) \left[\hat{h}_{KS} \phi_{\beta} \right](\mathbf{r}_g),$$

where h is the uniform grid-spacing.

Since the forces are the derivatives with respect to nuclear coordinate X_C , while our grid points are the electronic coordinates, x_g , we use the fact that for a basis function centered around \mathbf{R}_C , taking the derivative with respect to X_C is simply the negative of the derivative with respect to x evaluated at $\mathbf{r}_g - \mathbf{R}_C$:

$$\frac{\partial}{\partial X_C} \phi_{\alpha}(\mathbf{r}_g) = -\xi'_{\alpha}(x_g - X_C) \eta_{\alpha}(y_g - Y_C) \zeta_{\alpha}(z_g - Z_C),$$

such that derivatives can therefore also be defined inside a “window” surrounding the atom C and given as a product of three terms at each of its grid points. The grid is then used to evaluate the Pulay matrix elements of $\delta_C S$ and $\delta_C H$:

$$\left\langle \frac{\partial}{\partial X_C} \phi_{\alpha} \middle| \phi_{\beta} \right\rangle = h^3 \sum_{\mathbf{r}_g} \left[\frac{\partial}{\partial X_C} \phi_{\alpha}(\mathbf{r}_g) \right] \phi_{\beta}(\mathbf{r}_g),$$

$$\left\langle \frac{\partial}{\partial X_C} \phi_{\alpha} \middle| \hat{h}_{KS} \phi_{\beta} \right\rangle = h^3 \sum_{\mathbf{r}_g} \left[\frac{\partial}{\partial X_C} \phi_{\alpha}(\mathbf{r}_g) \right] \left[\hat{h}_{KS} \phi_{\beta} \right](\mathbf{r}_g),$$

The above Pulay terms are non-zero only when the ϕ_{α} basis belongs to atom C , i.e. when $\phi_{\alpha} \in C$, and therefore need to be calculated only for a very small number of α, β pairs, i.e. only when $\phi_{\alpha}, \phi_{\beta}$ have overlapping windows on the grid. The result of these conditions is that Pulay force matrices are incredibly sparse and their number of non-zero elements, $N_{\text{non zero}}$, is independent of the system size, as it depends only on the choice of basis set through the number of basis functions per atom. As for each degree of freedom (DOF), X_C (X direction of atom C), we have to compute a Pulay force sparse-matrix, we exploit these conditions in our code by only evaluating non-zero matrix elements and storing them in sparse-matrix structures. In Subsection IC we describe the method of storage and application (onto a vector) of the sparse structure we have used.

The algorithm for computing $\left(\frac{\partial S}{\partial X_C} \right)_{\alpha\beta}$

- For all basis functions $\alpha \in C$

- loop over all basis function $\beta < \alpha$ that overlap with α , then:
- If $\beta \in C$

$$\left(\frac{\partial S}{\partial X_C} \right)_{\alpha\beta} = \left\langle \frac{\partial}{\partial X_C} \phi_{\alpha} \middle| \phi_{\beta} \right\rangle + \left\langle \phi_{\alpha} \middle| \frac{\partial}{\partial X_C} \phi_{\beta} \right\rangle$$

- otherwise

$$\left(\frac{\partial S}{\partial X_C} \right)_{\alpha\beta} = \left\langle \frac{\partial}{\partial X_C} \phi_{\alpha} \middle| \phi_{\beta} \right\rangle$$

- For all basis functions $\alpha \notin C$

- loop over all basis function $\beta < \alpha$ that overlap with α , then:
- If $\beta \in C$

$$\left(\frac{\partial S}{\partial X_C} \right)_{\alpha\beta} = \left\langle \phi_{\alpha} \middle| \frac{\partial}{\partial X_C} \phi_{\beta} \right\rangle$$

- All other terms are not 0, and we do not store them in the sparse matrix structure.

(To simplify the code, as $\langle \phi_\alpha | \frac{\partial}{\partial X_C} \phi_\beta \rangle = \langle \frac{\partial}{\partial X_C} \phi_\beta | \phi_\alpha \rangle$, we always take the derivative from the left side).

Overall we get:

$$\left(\frac{\partial S}{\partial X_C} \right)_{\alpha\beta} = \begin{cases} \langle \frac{\partial}{\partial X_C} \phi_\alpha | \phi_\beta \rangle + \langle \phi_\alpha | \frac{\partial}{\partial X_C} \phi_\beta \rangle & \alpha, \beta \in C \\ \langle \frac{\partial}{\partial X_C} \phi_\alpha | \phi_\beta \rangle & \alpha \in C, \beta \notin C \\ \langle \phi_\alpha | \frac{\partial}{\partial X_C} \phi_\beta \rangle & \alpha \notin C, \beta \in C \\ 0 & \alpha, \beta \notin C \end{cases}$$

and the same can be done for the Hamiltonian Pulay terms:

$$\left(\frac{\partial H}{\partial X_C} \right)_{\alpha\beta}^{\text{Pulay}} = \begin{cases} \langle \frac{\partial}{\partial X_C} \phi_\alpha | \hat{h}_{KS} | \phi_\beta \rangle + \langle \phi_\alpha | \hat{h}_{KS} | \frac{\partial}{\partial X_C} \phi_\beta \rangle & \alpha, \beta \in C \\ \langle \frac{\partial}{\partial X_C} \phi_\alpha | \hat{h}_{KS} | \phi_\beta \rangle & \alpha \in C, \beta \notin C \\ \langle \phi_\alpha | \hat{h}_{KS} | \frac{\partial}{\partial X_C} \phi_\beta \rangle & \alpha \notin C, \beta \in C \\ 0 & \alpha, \beta \notin C \end{cases}$$

however, as the Hamiltonian includes terms that are explicitly dependent on nuclear coordinates in the form of the non-local (*nl*) and local (*loc*) pseudopotential terms: $\hat{v}_{pp}^{nl/loc} = \sum_{C' \in \text{nuclei}} \hat{v}_{pp(C')}^{nl/loc}$, there are also $\langle \phi_\alpha | \frac{\partial}{\partial X_C} \hat{h}_{KS} | \phi_\beta \rangle = \langle \phi_\alpha | \frac{\partial}{\partial X_C} \hat{v}_{pp}^{nl/loc} | \phi_\beta \rangle$ type terms that contribute to the overall force on atom C in the X direction. See Subsection IB below for the detail of these force terms.

B. The direct forces

Here we give the detail of calculating the $\langle \phi_\alpha | \frac{\partial}{\partial X_C} \hat{v}_{pp}^{nl/loc} | \phi_\beta \rangle$ type matrix elements.

Since the non-local and local pseudopotential operators are $\hat{v}_{pp}^{nl/loc} = \sum_{C' \in \text{nuclei}} \hat{v}_{pp(C')}^{nl/loc}$, the derivative with respect to a variation in nuclear coordinate X_C is given by:

$$\frac{\partial}{\partial X_C} \hat{v}_{pp}^{nl/loc} | \phi_\beta \rangle = \frac{\partial}{\partial X_C} \hat{v}_{pp(C)}^{nl/loc} | \phi_\beta \rangle.$$

The $\hat{v}_{pp(C)}^{nl/loc}$ operators have an analytical expression of the Kleinman-Bylander form [1], such that we can apply it, and its derivative, $\frac{\partial}{\partial X_C} \hat{v}_{pp(C)}^{nl/loc}$, on a vector on the grid.

Due to its short-range nature, $\hat{v}_{pp(C)}^{nl}$ and subsequently $\frac{\partial}{\partial X_C} \hat{v}_{pp(C)}^{nl}$ are stored on a small “window” of grid points around R_C . The $\langle \phi_\alpha | \frac{\partial}{\partial X_C} \hat{v}_{pp(C)}^{nl} | \phi_\beta \rangle$ matrix elements are therefore calculated as a multiplication of two grid vectors:

$$\left(\frac{\partial}{\partial X_C} V_{pp(C)}^{nl} \right)_{\alpha\beta}^{\text{direct}} = h^3 \sum_{\mathbf{r}_g \in (\alpha \cap \beta \cap \hat{v}_{pp(C)}^{nl})} \phi_\alpha(\mathbf{r}_g) \left[\left[\frac{\partial}{\partial X_C} \hat{v}_{pp(C)}^{nl} \right] \phi_\beta \right](\mathbf{r}_g), \quad (1)$$

where the sum over grid points \mathbf{r}_g is over only grid points that are inside the windows of all three terms, ϕ_α , ϕ_β and $\hat{v}_{pp(C)}^{nl}$. This requirement of overlapping windows for all three terms results in very sparse matrices, with the number of non-zero matrix elements, $N_{\text{non zeros}}$, dependent only on the choice of basis set and independent of system size.

For each degree of freedom (DOF), X_C (atom C in the X direction), we have to compute a $\frac{\partial}{\partial X_C} V_{pp(C)}^{nl}$ force sparse-matrix and apply it to a stochastic vector as part of the evaluation using the stochastic trace formula. In Subsection IC we describe the method of storage and application of the sparse structure we have used.

The algorithm for computing $\left(\frac{\partial}{\partial X_C} V_{pp(C)}^{nl}\right)_{\alpha\beta}^{direct}$

- loop over all basis functions β that have overlapping windows with $\hat{v}_{pp(C)}^{nl}$
 - Calculate the $\left[\frac{\partial}{\partial X_C} \hat{v}_{pp(C)}^{nl} \phi_\beta\right](\mathbf{r}_g)$ grid vector for all $\mathbf{r}_g \in \beta \cap \hat{v}_{pp(C)}^{nl}$
 - * loop over all basis functions α that overlap with both β , $\hat{v}_{pp(C)}^{nl}$
 - Calculate $\left(\frac{\partial}{\partial X_C} V_{pp(C)}^{nl}\right)_{\alpha\beta}$ according to Eq.(1)

The local PP operator, \hat{v}_{pp}^{loc} , (which includes the long range Coulomb attraction), depends directly on the density $n(\mathbf{r}_g)$. In this case, an equivalent method to the trace calculation of the direct $\frac{\partial}{\partial X_C} \hat{v}_{pp}^{loc}$ is done by usual planewaves calculations on the grid using $n(\mathbf{r}_g)$ in reciprocal space. This scaling of this approach is quadratic with system size when the forces on all atoms are calculated, however it is highly efficient.

C. Sparse matrix structures for Pulay and non-local PP forces

To exploit the sparsity of the above, direct and Pulay, force matrices, we do not store them in full $K \times K$ matrix structures (where K is the number of basis functions), but rather use compact a storage structure. In these, for every degree of freedom we store three lists of length $N_{\text{non zeros}}$: $(\text{val}, I, J) \equiv M_{ij}$ where (I, J) gives the location of the value, val , in the $K \times K$ matrix M .

$$M = \begin{pmatrix} 0 & \cdots & 0 & 0 \\ \vdots & \ddots & \vdots & \vdots \\ 0 & \cdots & a & b \\ 0 & \cdots & c & d \end{pmatrix}_{K \times K} \equiv \begin{pmatrix} \text{val} \\ a \\ b \\ c \\ d \end{pmatrix} \begin{pmatrix} I \\ K-1 \\ K-1 \\ K \\ K \end{pmatrix} \begin{pmatrix} J \\ K-1 \\ K \\ K-1 \\ K \end{pmatrix}$$

As per the above example, the sparse structure allows for a significant reduction in the number of stored values in memory as we only store $(3 \times N_{\text{non zeros}})$ elements per DOF as opposed to K^2 elements per DOF. Since the number of DOF's, $N_{\text{DOF}} \propto K$ and since $N_{\text{non zeros}}$ is a small number dependent only on the choice of basis set (but not on system size!) our sparse structure reduces the scaling of the memory requirement from $\mathcal{O}(K^3)$ to $\mathcal{O}(K)$.

The sparse structure also allows for an efficient matrix vector multiplication. For a matrix M and vector $|\mathbf{z}\rangle$ the operation

$$|\mathbf{y}\rangle = M |\mathbf{z}\rangle$$

is given by:

$$y_k = \sum_{n, I(n)=k} \text{val}(n) \times z_{J(n)}$$

such that we only require $N_{\text{non zeros}}$ multiplications for a matrix vector operation (as all terms of c , that are not in the I list, are zero).

For the stochastic trace formula we need to calculate expectation values using the stochastic vectors, χ . In a bra-ket notation, for a matrix M :

$$r = \langle \chi | M | \chi \rangle$$

is given by:

$$r = \sum_n^{N_{\text{non zeros}}} \chi_{I(n)} \times \text{val}(n) \times \chi_{J(n)}$$

such that we only require $2 \times N_{\text{non zeros}}$ multiplications. Since the calculation of the force operators' expectation values (direct and Pulay), per DOF, are independent of system size, the overall scaling of the force calculations using this sparse structure is $\mathcal{O}(K)$.

II. BASIC CONCEPTS IN STATISTICS

A. Random variables

In order to understand the statistical errors involved in our procedures we briefly review the concept of a random variable r [2]. It takes any one of a discrete set of values $\{r\}$ with a given probability $p(r) \geq 0$, where $\sum_r p(r) = 1$. The expected value of r is: $E[r] = \sum_r r p(r)$ and the variance is $\text{Var}[r] = E[(r - E[r])^2]$. Using a sample of I independent draws from the population of r 's we calculate the mean

$$m_I = \frac{1}{I} \sum_{i=1}^I r_i$$

and the standard deviation

$$s_I = \sqrt{\frac{1}{I-1} \sum_{i=1}^I (r_i - m_I)^2},$$

both can also be viewed as random variables with appropriate probability functions themselves. It can be shown that

1. The expected value of m_I is the same as that of r :

$$E[m_I] = E[r]$$

2. The variance of m_I is smaller by a factor I than that of r :

$$\text{Var}[m_I] = \frac{1}{I} \text{Var}[r]$$

3. The expected value of s_I^2 is equal to the variance of:

$$E[s_I^2] = \text{Var}[r].$$

From these properties, m_I and s_I^2 can serve as unbiased estimators of the expected value and variance of the original random variable. When I is sufficiently large, the interval of values $[m_I - \sigma_I, m_I + \sigma_I]$, where

$$\sigma_I = \frac{s_I}{\sqrt{I}}$$

is the uncertainty giving a 70% confidence interval for $E[r]$. Based on the sampled data, there is a probability of 70% that $E[r]$ falls within this interval.

B. Stochastic vectors

In section 2.4 of the main text we discuss the stochastic evaluation of observables using the stochastic trace formula

$$\text{Tr}[A] = E[\chi^T A \chi], \quad (2)$$

where we treat each $\chi^T A \chi$ as a random variable. The variance associated the result is given by

$$\text{Var}[\chi^T A \chi] = \frac{1}{2} \sum_{i \neq j} (A_{ij} + A_{ji})^2. \quad (3)$$

The relation in Eq. (2) is called the stochastic trace formula and it allows evaluating the trace of A by parameter estimation techniques based on statistical sampling theory.

Proof of Eq. (3) We begin the proof using the definition of the variance of a random variable, $\text{Var}[x] = \text{E}[x^2] - \text{E}[x]^2$, and considering $\chi^T A \chi$ as our random variable:

$$\begin{aligned} \text{Var}[\chi^T A \chi] &= \text{E}[(\chi^T A \chi)^T \chi^T A \chi] - (\text{E}[\chi^T A \chi])^2 \\ &= \text{E}[\chi^T A^T \chi \chi^T A \chi] - (\text{Tr}[A])^2 \\ &= \text{E}[\chi_k \chi_l \chi_i \chi_j] A_{kl} A_{ij} - (\text{Tr}[A])^2 \end{aligned} \quad (4)$$

where in the second line we have used Eq. (2), and in the third line the fact that the matrix A is completely deterministic. We will now evaluate $\text{E}[\chi_k \chi_l \chi_i \chi_j]$, using that $\text{E}[\chi_i \chi_j] = \delta_{ij}$:

$$\begin{aligned} \text{E}[\chi_k \chi_l \chi_i \chi_j] &= \delta_{kl} \text{E}[\chi_i \chi_j] + (1 - \delta_{kl}) (\delta_{ki} \text{E}[\chi_l \chi_j] + (1 - \delta_{ki}) (\delta_{kj} \text{E}[\chi_i \chi_l])) \\ &= \delta_{kl} \delta_{ij} + (1 - \delta_{kl}) (\delta_{ki} \delta_{lj} + (1 - \delta_{ki}) \delta_{kj} \delta_{il}) \\ &= \delta_{kl} \delta_{ij} + \delta_{ki} \delta_{lj} + \delta_{kj} \delta_{il} - 2 \delta_{kl} \delta_{kj} \delta_{il} \end{aligned}$$

and multiply by $A_{kl} A_{ij}$ and sum over all indices:

$$\begin{aligned} \text{E}[\chi_k \chi_l \chi_i \chi_j] A_{kl} A_{ij} &= A_{kk} A_{ii} + A_{ij} A_{ij} + A_{ji} A_{ij} - 2 A_{ii}^2 \\ &= \text{Tr}[A]^2 + \sum_{i \neq j} A_{ij} (A_{ij} + A_{ji}) \\ &= \text{Tr}[A]^2 + \frac{1}{2} \sum_{i \neq j} (A_{ij} + A_{ji})^2 \end{aligned}$$

Substituting back into Eq. (4), we arrive at

$$\text{Var}[\chi^T A \chi] = \frac{1}{2} \sum_{k \neq l} (A_{kl} + A_{lk})^2$$

C. Parameter estimation and statistical errors

Often expected value $\text{E}[r]$ of a distribution of a random variable r is not known. The estimation of this parameter can be done, based on the use of a finite sample r_i of size I , as discussed in section II A. As an demonstration of this procedure we return to the question of how to evaluate the $\text{Tr}[A]$. We take a sample of I stochastic vectors χ_i and form a random variable $\frac{1}{I} \sum_{i=1}^I \chi_i^T A \chi_i$. Then

$$\text{Tr}[A] = \text{E} \left[\frac{1}{I} \sum_{i=1}^I \chi_i^T A \chi_i \right], \quad (5)$$

and

$$\text{Var} \left[\frac{1}{I} \sum_{i=1}^I \chi_i^T A \chi_i \right] = \frac{1}{2I} \sum_{k \neq l} (A_{kl} + A_{lk})^2.$$

As discussed above, the sample mean $m_I = \frac{1}{I} \sum_{i=1}^I \chi_i^T A \chi_i$ and corresponding standard deviation s_I can be used to provide a confidence interval of uncertainty $\sigma_I = s_I / \sqrt{I}$ for the value of $\text{Tr}[A]$. This statistical approach, of building a confidence interval for $\text{Tr}[A]$ involves I applications of A to a vector, whereas the deterministic calculation of $\text{Tr}[A]$ involves K such applications. Therefore, as long as $I \ll K$ we obtain a large saving in the numerical effort, but at the price of introducing an uncertainty.

Now, suppose we wanted to estimate a given function of the expected value of a random variable, $f(\text{E}[r])$. The simplest procedure is apply f to the sample mean m_I and take $f(m_I)$ as such an estimate. This procedure works when $f(x)$ is a linear function of x but otherwise will generally incur a systematic error, called a bias. For example, when $f(x) = x^2$ and r is a random variable with $\text{E}[r] = 0$ and $\text{Var}[r] = 1$, then $\text{E}[f(m_I)] = \text{E}[m_I^2] = \frac{\text{E}[r^2]}{I} = \frac{1}{I}$ which is clearly different from the exact value of $f[\text{E}[r]] = \text{E}[r]^2 = 0$. Hence we have the undesirable case, that for a finite value of I , errors will involve fluctuations around the wrong value. Note however, that as I grows, the bias diminishes in proportion to $\frac{1}{I}$. To be useful, when a bias exists, we need to make sure it is of sufficiently small magnitude.

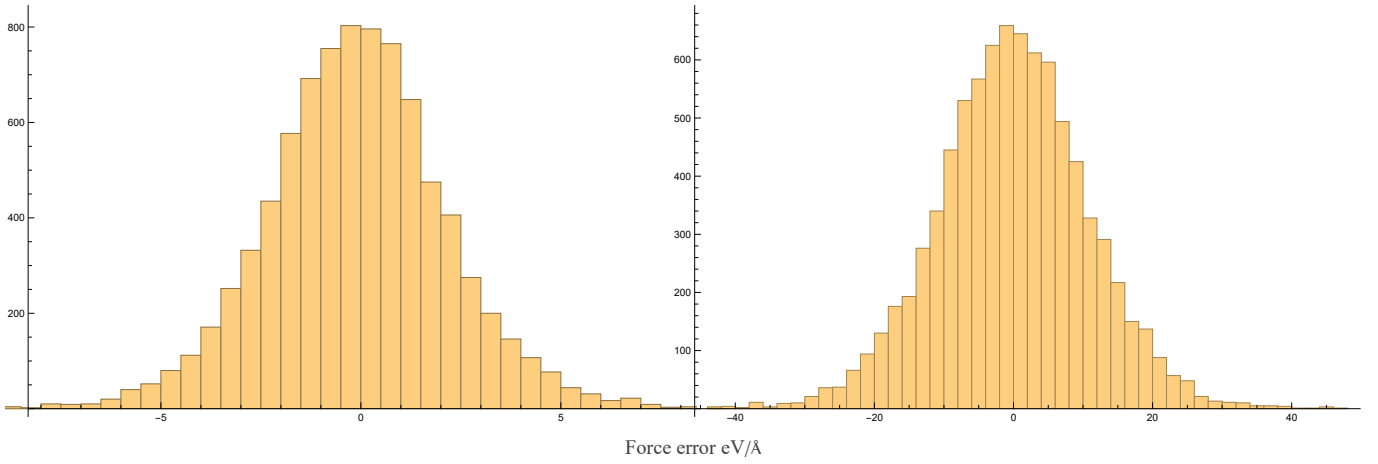


Figure 1. Histograms representing the distribution in the errors in the sDFT forces with $I = 12$ stochastic vectors. We show the errors of forces acting on two nitrogen atoms from the solvated-TrpZip2 system. On the left (right) panel is the data for the smallest (largest) standard deviation cases from all nitrogen atoms. The data for the histogram was collected by repeating the sDFT force calculation $M = 2800$ times and comparing the force vector \mathbf{F}_C^m on each atom C to the corresponding deterministic (accurate) value \mathbf{F}_C^{dDFT} . Thus we obtained $3 \times M$ error values in the x-y-z components of the force, which represent the scatter of force components for the atom.

D. Distribution of random errors in the forces

In Fig. 1 we present histograms of the sDFT force errors ($\mathbf{F}_C^m - \mathbf{F}_C^{dDFT}$, $m = 1, \dots, M$) on two nitrogen atoms in the solvated-TrpZip2 system. We selected the atoms that have the smallest/largest standard deviation. For both atoms, we find a Gaussian-looking distribution of the force errors centered around zero with a standard deviation within the bounds reported in the Manuscript.

III. EMBEDDED FRAGMENTS

A. Calculation detail in the sDFT code

We would like to explain here how the equation:

$$\langle \hat{o} \rangle_I^{EF} = \langle \hat{o} \rangle_I + \sum_f \langle \Delta \hat{o}^f \rangle_I \quad (6)$$

is implemented within our sDFT code. We give here the steps in the calculation of the correction terms from each fragment, $\langle \Delta \hat{o}^f \rangle_I$, where we defined the fragment-based correction as the difference between the dDFT and sDFT, for every fragment:

$$\langle \Delta \hat{o}^f \rangle_I = \langle \hat{o}^f \rangle_{dDFT} - \langle \hat{o}^f \rangle_I$$

For the calculation of $\langle \hat{O} \rangle_{dDFT}^f$ we solve the generalised eigenvalue problem, find P^f , the density matrix of the fragment subsystem, and trace:

$$\langle \hat{o} \rangle_{dDFT}^f = 2 \text{Tr} \left[(OP)^f \right] \quad (7)$$

while $\langle \hat{o} \rangle_I^f$ is calculated using the stochastic trace formula:

$$\langle \hat{o} \rangle_I^f = 2 \frac{1}{I} \sum_{i=1}^I (\chi_i^T)^f (OP)^f \chi_i^f$$

with the vectors χ_i^f that are “cut-outs” of the vectors χ_i which we use in the stochastic trace formula for the full system, such that the stochastic element in the fragment calculation corresponds with the one made on the full system. Rearranging the above equation to be written as a trace expression gives:

$$\langle \hat{o} \rangle_I^f = 2 \text{Tr} \left[(OP)^f \left(\frac{1}{I} \sum_{i=1}^I \chi_i^f (\chi_i^T)^f \right) \right]$$

Finally, for the deterministic trace of Eq. (7) we multiply $(OP)^f$ by $(\text{Id})^f$, the identity matrix of the fragment dimensions, which allows us to rewrite the fragment correction as:

$$\langle \Delta \hat{o}^f \rangle_I = 2 \text{Tr} \left[(OP \Delta_I)^f \right]$$

where $\Delta_I^f = (\text{Id})^f - \frac{1}{I} \sum_{i=1}^I \chi_i^f (\chi_i^T)^f$.

B. Another look at the fragments

A second useful outlook on the embedded-fragments method gives insight into the reason the statistical errors are reduced when the method is used. We rearrange Eq. (6) to get:

$$\begin{aligned} \langle \hat{o} \rangle_I^{EF} &= \sum_f \langle \hat{o} \rangle_{\text{dDFT}}^f + \left[\langle \hat{o} \rangle_I - \sum_f \langle \hat{o} \rangle_I^f \right] \\ &= 2 \text{Tr}^{\text{det}} \left[\sum_f (OP)^f \right] + 2 \text{Tr}^{\text{stoch}} \left[O \left(P - \sum_f P^f \right) \right] \end{aligned} \quad (8)$$

such that $\text{Tr}^{\text{stoch}} \left[O \left(P - \sum_f P^f \right) \right]$ is a stochastic correction to the dDFT calculation summed over all fragments. As per Eq. (3) the variance in the stochastic trace is given by the magnitude of the off-diagonal matrix elements of $O \left(P - \sum_f P^f \right)$, and so clearly, as $\sum_f P^f$ approaches P the stochastic trace will have much smaller variance.

IV. SYSTEM SIZE DEPENDENCY

We compare the statistical errors of sDFT forces of two Trp-*zip2* peptide systems, each with a different number of solvating water molecules. The first is the system we presented results for in Section III of the manuscript, solvated by 425 water molecules, while the second is a smaller system, with only 195 solvating water molecules. To keep the systems as similar as possible we cropped the smaller system directly from the larger one, such that the 195 solvating water molecules that are closest to the peptide are identical in their geometry in both systems, and the embedded-fragment method was employed such that, for both systems, the entire peptide composes one fragment, while the remaining water molecules are split into fragments with an average number of 16 water molecules per fragment.

In Fig. 2 we present the uncertainty and bias estimates for the sDFT forces on the 20 nitrogen atoms of the peptide, in the two systems described above, for the case of $I = 12$ stochastic orbitals. To allow for a comparison of the bias estimates, we repeated the calculation a large, $M = 2800$, times. The uncertainty values of each nitrogen atom are near identical between the two systems. Since the errors fluctuate, even for 2800 repetitions, we compare the median value over all nitrogen atoms, and find that it is practically identical for the two systems. These results give indication to a weak dependency of the statistical errors, uncertainty and bias, on system size.

V. COMPARISON WITH REAL-SPACE GRID REPRESENTATION

We have checked the speed of basis sets vs. real-space grid calculations (as described in Ref. [3]) with $\text{Si}_{35}\text{H}_{36}$ as a benchmark. For the real-space grid calculations we used a grid of 64^3 points of spacing $\delta x = 0.5a_0$ and the wall time for the real-space sDFT/SCF iteration was one minute. For the basis-set sDFT calculation we used the same integration grid.

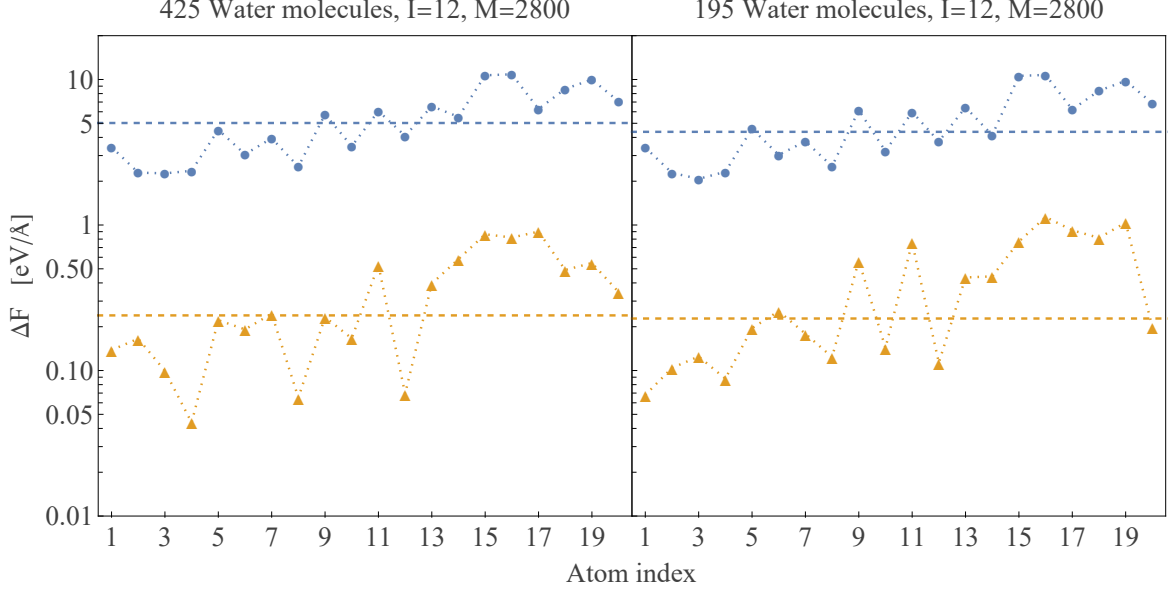


Figure 2. The statistical errors in the sDFT forces acting on the 20 nitrogen atoms in two solvated-TrpZip2 systems (using 425 solvating water molecules on the left and 195 on the right). Forces for both systems were calculated using $I = 12$ stochastic vectors. For each Nitrogen atom, we show the uncertainty σ_C (blue dots), and the estimate in the bias $\Delta\rho_C$ (orange triangles), see Eqs. 27 – 28 in manuscript. The dotted lines connecting the markers are presented as a guide for the eye, while the dashed horizontal lines are medians over all atoms of σ_C and $\Delta\rho_C$.

	Relative speed of Hamiltonian operation	Relative Chebyshev expansion length	Relative speed	Relative statistical error in force	Relative required number of CPUs	Relative wall-time	
	v_H	N_C	$v = \frac{v_H}{N_C}$	δf	$N_p = \delta f^2$	Running on the same number of processors N_p/v	Running on N_p times more processors $1/v$
STO-3G	40	0.08	500	1.4	2	0.004	2×10^{-3}
6-31G	4	0.13	31	4.6	21	0.700	3×10^{-2}
Real space	1	1	1	1	1	1	1

Table I. Data for comparing speeds and wall times for real-space and basis-set calculations

Here are the results of our analysis (summarized in Table I): the Hamiltonian operation for STO-3G and 6-31G are a factor 40 and 4 respectively faster than that of the real-space grid. Furthermore, the energy range of the basis sets is much smaller, so the Chebyshev expansion length of STO-3G and 6-31G are a factor 13 and 8 shorter than that of the real space grid. As a result, the operation of the DM on a vector in STO-3G and 6-31G are a factor of about 500 and 30 faster respectively than in the real-space grid calculation. Therefore, the calculation of a single SCF iteration is much faster in the basis set calculations than in the real-space grid.

Next, we considered the fluctuation error in both calculations. Surprisingly, we found, that the standard deviation of a typical force component on Si, for the STO-3G and the 6-31G basis sets are larger by a factor 1.4 and 4.6 respectively than that for the real-space grid. This means that for a given standard deviation goal, the basis set calculations will require more CPUs by factors of about $N_p = 1.4^2 \approx 2$ and $N_p = 4.6^2 \approx 21$, respectively, than the grid calculation.

Summarizing, STO-3G calculations can be very fast relative to the real-space grid's, however, it is well known that STO-3G is not accurate enough to be a reliably useful basis. When run with the same number of processors, the overall numerical effort of the 6-31G basis is comparable to that of the real-space grid calculation. However, if one can allocate a factor of $N_p \approx 21$ more processors to the 6-31G calculation than needed by the real-space grid, the

overall speed of the former will be 30 times faster.

-
- [1] L. Kleinman and D. M. Bylander, Phys. Rev. Lett. **48**, 1425 (1982).
 - [2] A. Papoulis and S. U. Pillai, *Probability, random variables, and stochastic processes*, 4th ed. (McGraw-Hill, Boston, 2002).
 - [3] E. Arnon, E. Rabani, D. Neuhauser, and R. Baer, The Journal of Chemical Physics **146**, 224111 (2017).